JACS ARTICLES

Published on Web 07/22/2009

Triplet States of the Nonlinear Optical Chromophore DCM in Single Crystals of Potassium Hydrogen Phthalate and Their Relationship to Single-Molecule Dark States

Antonio Barbon,[†] Eric D. Bott,[‡] Marina Brustolon,*[,†] Marianna Fabris,[†] Bart Kahr,*[,‡] Werner Kaminsky, Philip J. Reid,*[,‡] Susanna M. Wong,[‡] Kristin L. Wustholz,[‡] and Roberto Zanré[†]

Dipartimento di Scienze Chimiche, Università degli Studi di Padova, via Marzolo 1, 35131 Padova, Italy, and Department of Chemistry, University of Washington, Box 351700, Seattle, Washington 98915-1700

Received April 29, 2009; E-mail: bart.kahr@nyu.edu

Abstract: Single-molecule dark states are often attributed to photoexcited triplets with scant evidence of the participation of paramagnetic molecules. The photodynamics of blinking single molecules of 4-dicyanomethylene-2-methyl-6-*p*-dimethylaminostyryl-4H-pyran (DCM) in crystals of potassium hydrogen phthalate (KAP) were compared with the lifetimes of DCM triplet states, likewise in KAP, whose zero-field splitting (ZFS) tensors were fully characterized by time-resolved electron paramagnetic resonance (TR-EPR) spectroscopy. Luminescent mixed crystals of KAP were grown from solutions containing 10^{-4} -10^{-9} M DCM, a model optically nonlinear chromophore. The luminescent dye was localized in the $\{11\bar{1}\}$ crystalline growth sectors. The photoexcited triplets states of DCM in the heavily dyed (10^{-4} M) crystals were analyzed by TR-EPR spectroscopy. The photoexcited singlet states of DCM in lightly dyed crystals (10^{-9} M) were analyzed by single-molecule microscopy. Large blue shifts in the absorption and emission spectra of DCM in KAP were interpreted as a consequence of protonation at the dimethylamino nitrogen atom, an assignment supported by calculations of the zero-field splitting (ZFS) tensors of molecules in their triplet states. Experimental ZFS tensors with eigenvalues comparable to those of the computed tensors were determined from the angular dependence of the EPR spectra of $DCMH^+$ triplets within KAP single crystals with respect to the applied magnetic field. Data from individual growth sectors failed to show magnetically equivalent site occupancies, evidence of the kinetic ordering during growth. The intermittent fluorescence of individual chromophores was analyzed. The distributions of on(off) times were characterized by distributed rates fit to power laws. The lifetime of the triplet states was analyzed from the time decay of the EPR signals between 100 and 165 K. The data were well fit with a single time constant for the signal decay, a result wholly inconsistent with the blinking of single molecules with off times commonly of tens of seconds. Triplet decay was extrapolated to ~25 μs at room temperature. Therefore, the assumption that single-molecule dark states originate with triplet excited states is not sustainable for single DCM molecules in KAP.

Introduction

Single-molecule spectroscopy is one of the truly transformative themes in 21st century chemistry. Scientists first learned to parse the inhomogeneous broadening of ensemble-averaged spectral bands into their single-molecule components during investigations of mixed crystals.[1] Subsequently, single molecules have been observed in all manner of complex media,[2] yet the organization[3] and photodynamical behavior of single molecules,[4] even in single-crystal hosts, can be surprisingly complex.

Single-molecule emission is commonly analyzed by its time dependence during continuous photoexcitation. A common signature of single molecules is emission intermittency or 'blinking'.[5] Histograms of the lengths of emissive (on times) and nonemissive periods (off times) have been described by exponential functions ostensibly reflecting the rate of intersystem crossing ($S_1 \rightarrow T_1$) and the decay rate of the triplet state ($T_1 \rightarrow S_0$). However, the blinking of other systems cannot readily be assigned to population and depopulation of an optically dark state with well-defined rate constants.[6] Triplet intermediates have often been invoked because the rate constants associated with

* Present address: Department of Chemistry, New York University, 100 Washington Square East, New York, NY 10003.
[†] Università degli Studi di Padova.
[‡] University of Washington.

(1) Moerner, W. E; Kador, L *Phys. Rev. Lett.* **1989**, *62*, 2535–2538. Kador, L.; Horne, D. E.; Moerner, W. E. *J. Phys. Chem.* **1990**, *94*, 1237–1248. Orrit, M.; Bernard, J. *Phys. Rev. Lett.* **1990**, *65*, 2716–2719. Ambrose, W. P.; Basché, Th.; Moerner, W. E *J. Chem. Phys.* **1991**, *95*, 7150–7163.
(2) Wang, C.; Bai, C. *Single Molecule Chemistry and Physics: An Introduction*; Springer: Dordrecht, 2006; Chapters 8 and 9.
(3) Wustholz, K. L; Kahr, B; Reid, P. J *J. Phys. Chem. B* **2005**, *109*, 16357–16362.
(4) (a) Wustholz, K. L.; Bott, E. D.; Isborn, C. M.; Li, X.; Kahr, B.; Reid, P. J. *J. Phys. Chem. C* **2007**, *111*, 9146–9156. (b) Wustholz, K. L.; Sluss, D. R. B.; Kahr, B.; Reid, P. J. *Int. Rev. Phys. Chem.* **2008**, *27*, 167–200. (c) Wustholz, K. L.; Bott, E. D.; Kahr, B.; Reid, P. J. *J. Phys. Chem. C.* **2008**, *112*, 7877–7885.
(5) Dickson, R. M; Cubitt, A. B; Tsien, R. Y; Moerner, W. E. *Nature* **1997**, *388*, 355–358. Moerner, W. E. *Science* **1997**, *277*, 1059–1060.

10.1021/ja903284y CCC: $40.75

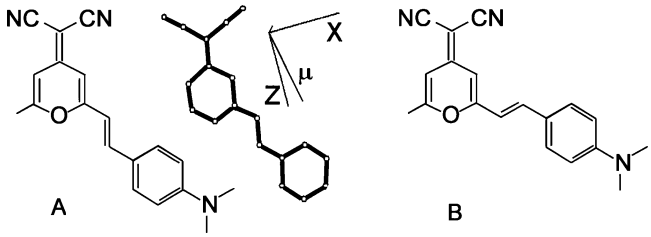

Figure 1. Schematic molecular structure of DCM in two delimiting conformations A and B. Shown next to A is the optimized triplet state geometry of $DCMH^+$ and vectors corresponding the ZFS eigendirections and the first excited state electric dipole transition moment. Only atoms carrying π-spin density in $DCMH^+$ are shown.

dark-state depopulation are consistent with typical triplet lifetimes.[7] Stronger evidence for triplets comes from the phosphorescence[8] and the optically detected magnetic resonance of single molecules.[9] However, to the best of our knowledge, there is little overlap between systems for which triplet-state population and decay has been evidenced and systems for which fluorescence intermittency has been analyzed. A stronger connection between triplet states and dark states remains to be established.

An alternative assignment for the dark state is the formation of a molecular radical ion produced by electron transfer to the surroundings. This explanation was first advanced by Zondervan et al. in their studies of rhodamine 6G (R6G) embedded in polyvinyl alcohol.[10] Specifically, an EPR spectrum of this composite material obtained during optical excitation resonant with that of R6G contained a transition corresponding to $g = 2$ consistent with the formation of a spin-1/2 radical. This experiment is the only correlation of radical formation and single-molecule blinking dynamics and is routinely invoked to support electron-transfer processes as being responsible for dark-state formation in a variety of other molecular systems. The generality of electron-transfer-mediated blinking dynamics remains to be explored.

Here, we report single-molecule microscopy of the luminophore 4-dicyanomethylene-2-methyl-6-*p*-dimethylaminostyryl-4H-pyran (DCM, Figure 1) in single crystals of potassium hydrogen phthalate (conventionally abbreviated KAP for potassium acid phthalate, $C_6H_4{\cdot}COOH{\cdot}COO^-K^+$, space group $Pca2_1$) in conjunction with time-resolved electron paramagnetic resonance (TR-EPR) of the photoexcited triplet states. Observations were also made on the isomorphous rubidium hydrogen phthalate (RAP). We show to what extent the orientations of the chromophores determined by magnetic resonance are consistent with orientations determined by single-molecule fluorescence polarization microscopy, and likewise to what extent the lifetimes of *bona fide* triplets observed directly by EPR can be reconciled with the dark-state kinetics.

DCM (Figure 1) is efficient in laser gain media,[11] as a solar concentrator,[12] and is a model nonlinear optical chromophore.[13] It undergoes a large change in dipole moment upon excitation,[14] giving rise to solvatochromism[15] that is further complicated by *cis*−*trans* photoisomerism[16] and the possibility of so-called twisted intramolecular charge transfer (TICT) states.[17] The photophysical properties of DCM have been reported in a variety of condensed media including lipids,[18] polymers,[19] glasses,[20] and zeolites.[21] We observed that KAP/DCM (this notation used throughout indicates a KAP crystal doped with small quantities of DCM) exhibits up-conversion luminescence.[22]

Moerner and co-workers observed single DCM molecules in PMMA.[23] We previously reported the determination of the orientations of single DCM molecules in KAP crystals[3] and during electric field poling of doped polymers.[24] While DCM remains a popular analyte for single-molecule microscopy, the dynamics of its triplet state have not been studied in parallel with the photodynamics of its dark state. The triplet state of DCM has never been reported so far, but we have observed it in KAP/DCM. This contribution addresses the invocation of triplet states and radical formation as the etiology of blinking.

Experimental Section

Crystal Growth and Bulk Characterization. All chemicals were purchased from Aldrich and used without further purification. Rubidium hydrogen phthalate (RAP) was prepared by mixing stoichiometric quantities of RbOH and phthalic acid in water.

KAP and RAP were dissolved in deionized water (Barnstead NANOpure, 18.2 MΩ cm^{-1}). DCM was dissolved in a minimal quantity of ethanol prior to addition to the aqueous crystal-growth solution (110 g/L KAP). KAP crystals grow by spontaneous nucleation at room temperature as {010} plates with the following

(6) Orrit, M; Bernard, J. *Phys. Rev. Lett.* **1990**, *65*, 2716–2719. Basché, T.; Kummer, S.; Brauchle, C. *Nature* **1995**, *373*, 132–134. Yip, W. T.; Hu, D. H.; Yu, J.; Vanden Bout, D. A.; Barbara, P. F. *J. Phys. Chem. A* **1998**, *102*, 7564–7575. Kulzer, F.; Kummer, S.; Basché, T.; Bräuchle, C. *J. Inf. Rec.* **1996**, *22*, 567–572. Veerman, J. A.; Garcia-Parajo, M. F.; Kuipers, L.; van Hulst, N. F. *Phys. Rev. Lett.* **1999**, *83*, 2155–2158. Bernard, J.; Fleury, L.; Talon, H.; Orrit, M. *J. Chem. Phys.* **1993**, *98*, 850–859. Köhn, F.; Hofkens, J.; Gronheid, R.; Van der Auweraer, M.; De Schryver, F. C. *J. Phys. Chem. A* **2002**, *106*, 4808–4814.
(7) See for example: Fu, Y; Zhang, J.; Lakowicz, J. R. *Langmuir* **2008**, *24*, 3429–3433. Gensch, T.; Böhmer, M.; Aramendía, P. F. *J. Phys. Chem. A* **2005**, *109*, 6652–6658. Haase, M.; Hübner, C. G.; Reuther, E.; Herrmann, A.; Müllen, K.; Basché, Th. *J. Phys. Chem. B* **2004**, *108*, 10445–10450.
(8) Mei, E.; Vinogradov, S.; Hochstrasser, R. M. *J. Am. Chem. Soc.* **2003**, *125*, 13198–13204. Brown, R.; Wrachtrup, J.; Orrit, M.; Bernard, J.; von Borczyskowski, C. *J. Chem. Phys.* **1994**, *100*, 7182–7191.
(9) Köhler, J; Disselhorst, J. A. J. M.; Donckers, M. C. J. M.; Groenen, E. J. J.; Schmidt, J.; Moerner, W. E. *Nature* **1993**, *363*, 242–244. Wrachtrup, J.; von Borczyskowski, C.; Bernard, J.; Orrit, M.; Brown, R. *Nature* **1993**, *363*, 244–245.
(10) Zondervan, R.; Kulzer, F.; Orlinskii, S. B.; Orrit, M. *J. Phys. Chem. A* **2003**, *107*, 6770–6776.
(11) Hammond, P. R. *Opt. Commun.* **1979**, *29*, 331–333. Marason, E. G. *Opt. Commun.* **1981**, *37*, 56–58. Antonov, V. S.; Hohla, K. L. *Appl. Phys. B: Laser Opt.* **1983**, *32*, 9–14.
(12) Taleb, A. M.; Chiad, B. T.; Sadik, Z. S. *Renewable Energy* **2005**, *30*, 393–398.
(13) Moylan, C. R.; Ermer, S.; Lovejoy, S. M.; McComb, I.-H.; Leung, D. S.; Wortmann, R.; Krdmer, P.; Twieg, R. J. *J. Am. Chem. Soc.* **1996**, *118*, 12950–12955.
(14) Meyer, M.; Mialocq, J. C. *Opt. Commun.* **1987**, *64*, 264–268.
(15) Mialocq, J. C.; Meyer, M. *Laser Chem.* **1990**, *10*, 277–296.
(16) Drake, J. M.; Lesiecki, M. L.; Camaioni, D. M. *Chem. Phys. Lett.* **1985**, *113*, 530–534.
(17) Meyer, M.; Mialocq, J. C.; Perly, B. *J. Phys. Chem.* **1990**, *94*, 98–104. Marguet, S.; Mialocq, J. C.; Millie, P.; Berthier, G.; Momicchioli, F. *Chem. Phys.* **1992**, *160*, 265–279.
(18) Coutinho, P. J. G.; Castanheira, E. M. S.; Rei, M. C.; Elisabete, M.; Oliveira, C. D. R. *J. Phys. Chem. B* **2002**, *106*, 12841–12846.
(19) Bondarev, S. L.; Knyukshto, V. N.; Stepuro, V. I.; Stupak, A. P.; Turban, A. A. *J. Appl. Spectrosc.* **2004**, *71*, 194–201.
(20) Hu, W.; Ye, H.; Li, C.; Jiang, Z.; Zhou, F. *Appl. Opt.* **1997**, *36*, 579–583.
(21) Guo, H.; Zhang, X.; Aydin, M.; Xu, W.; Zhu, H.-R.; Akins, D. L. *J. Mol. Struct.* **2004**, *689*, 153–158.
(22) Benedict, J. B.; Wallace, P. M.; Reid, P. J.; Jang, S.-H.; Kahr, B. *Adv. Mater.* **2003**, *15*, 1068–1070.
(23) Paige, M. F.; Bjerneld, E. J.; Moerner, W. E. *Single Mol.* **2001**, *2*, 191–201.
(24) Wallace, P. M.; Sluss, D. R. B.; Dalton, L. R.; Robinson, B. H.; Reid, P. J. *J. Phys. Chem. B* **2006**, *110*, 75–82.

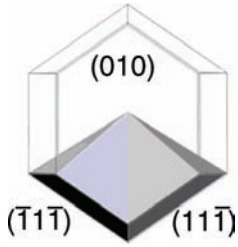

Figure 2. KAP habit with DCM-doped sectors delineated (shaded).

additional forms: {111}, {11$\bar{1}$}, {110}, and occasionally {12$\bar{1}$} (Figure 2). DCM had little effect on the habit of KAP under the conditions studied. At concentrations of DCM > 10^{-4} M, the aspect ratio (*c*/*a*) of the resulting mixed crystals was reduced. The absolute sense of the polar [001] axis, to which all (*hkl*) indices refer, was assigned by anomalous scattering of X-rays.[25]

Heavily dyed crystals were grown from ~0.1 mM dye solutions and characterized using polarized absorption microspectrophotometry (Olympus BX-50 microscope coupled to a Si-Photonics 440 spectrometer) and fluorescence spectroscopy (Spex FluoroMax-2). The segregation coefficient (σ_{seg}), defined as the mole ratio of dye in the crystal to dye in the growth solution, was determined by absorbance measurements of redissolved crystals. For heavily dyed crystals of KAP/DCM, σ_{seg} is ~0.4%, corresponding to approximately 1 dye molecule per 10,000 KAP molecules. Mixed crystals of KAP/DCM and RAP/DCM with chromophore densities suitable for single-molecule investigations were grown from ~5 nM dye solutions.

Crystals of DCM were grown by slow evaporation of an ethanol solution containing an equimolar amount of phthalic acid. Crystals were indexed with Nonius KappaCCD diffractometer at 295 K. Data was collected using Mo Kα radiation (λ = 0.71073 Å). Integration of intensities and cell refinement was carried out using HKL2000[26] and HKL SCALEPACK, respectively. The structure was solved by direct methods (SIR97)[27] in the orthorhombic space group *C*2/*c*. The structure solution gave a complete heavy atom phasing model consistent with the proposed structure. Structures were refined using SHELXL-97.[28] Non-hydrogen atoms were refined anisotropically by full-matrix least-squares. All hydrogen atoms were refined with a riding model.

Single-Molecule Microscopy. Single molecules were studied with an inverted confocal microscope described in detail elsewhere.[3,4] Dyed KAP crystals were mounted on a scan stage (Queensgate, NPS-XY-100B) and photoexcited at low power (<10 μW) using a 488-nm (Novalux, Protera) or 405-nm (Photonic Products, PM-MF108-4) solid-state diode laser. The excitation field was filtered (Chroma, D405), reflected toward the sample using an appropriate dichroic mirror (Chroma, Z488RDC or Z405RDC), and focused to a diffraction-limited spot using a 100× oil-immersion objective (Nikon, PlanFluor 1.3 NA). Epifluorescence was collected from the sample, passed through the dichroic mirror, an emission filter (Chroma, HQ510/LP for 488-nm excitation and HQ435/LP for 405-nm excitation), and a confocal pinhole (CVI, 75-μm diameter). Emission was detected using a single-photon-counting avalanche photodiode (PerkinElmer, SPCM-AQR-16).

Total emission intensity following linearly polarized excitation modulated with a half-waveplate (CVI Laser) between the [100] and [001] crystal eigenmodes was measured over a 10 × 10 μm^2 area by scanning the sample in 100-nm steps with 100-ms integration time per point. Reported values of θ were defined with respect to [100] in the *ac*-plane. Single-molecule-emission time traces were collected for 100 s, employing a 50-ms integration time per point. Data collection was accomplished using LabVIEW (National Instruments) software.

Molecular transitions between emissive (on) and nonemissive (off) states, commonly referred to as blinking, were distinguished by thresholding.[29] Setting the proper threshold is critical to accurately quantify blinking that occurs over multiple time scales since both fast and slow blinking can be obscured by setting a threshold that is artificially or carelessly assigned.[34] Single-molecule-emission time traces in KAP/DCM were analyzed employing a threshold between the highest-intensity state (I_{on}) and the background intensity (I_{off}) typically ~20 counts per 50 ms. Threshold values corresponding to the average between the mean on and off intensities (i.e.,($\langle I_{on}\rangle + \langle I_{off}\rangle$)/2) were employed. The intensity at a given time above and below the threshold value was set to 1 and 0, respectively. A 'switch' was defined as a transition from 1 to 0, or vice versa. The fastest measurable switching rate is 0.05 s^{-1}. On(off) times were defined as the temporal duration of successive on (off) events prior to a switch. All data were evaluated with thresholds corresponding to 20% below and above $\langle I_{on}\rangle$ and $\langle I_{off}\rangle$, respectively. The on(off) time probability densities ($P(\tau_{on/off})$) were computed by compiling histograms of the on(off) times for many molecules and dividing each value in the distribution by the average time to its nonzero nearest neighbors.[29] Single molecules that did not switch and that switched just once, and permanent off events corresponding to molecular photobleaching were not included in the analyses. Data from 44 single molecules containing 4402 emissive events and 4395 nonemissive events were combined in the analysis.

Recently, Yang and co-workers presented an algorithm for the detection of discrete change points in emission intensity traces from single emitters.[30] In this so-called change-point detection (CPD) approach, temporal-emission traces were analyzed in a statistically unbiased and systematic fashion. Incoming photons and detector noise were modeled as Poisson distributed. Intensity change points were detected through a generalized likelihood ratio test. The probability that a change point occurred at a given time was calculated and compared to the probability of no change point. Initially, the *n* detected change points denote $n + 1$ unique intensity levels, which were grouped together using another likelihood ratio calculation comparing the probability of assigning any two intensity levels to a single emission state. The true number of states is determined through Bayesian information criterion that weighs the marginal information increase upon the inclusion of another on state against the penalty of adding extra adjustable parameters. Ultimately, the CPD method reports the change-point locations as well as the number and temporal durations of intensity levels (i.e., emission states).

Time-Resolved Electron Paramagnetic Resonance. The TR-EPR signals generated from photoexcited triplet states of DCM in KAP were produced by photoexcitation of the sample with a Brilliant Quantel Nd:YAG laser equipped with a third harmonic generator (355 nm). Pulses were 5 ns wide with energy at the sample of 3.5 mJ per shot at ~10 Hz. The light was conveyed into the cavity through an optical window in the cryostat (Oxford CF935) of a Bruker ELEXYS X-band EPR spectrometer equipped with a high quality factor (*Q*) dielectric cavity. The EPR signal obtained under continuous microwave irradiation was recorded after the laser flash by a digital oscilloscope (LeCroy 9361). The response time of the apparatus was 600−800 ns.

Integration with time windows of around 500 ns produced slices along the field at the maximum of the transient signal (~700 ns after the laser flash). The photoexcitation produces spin-polarized

(25) Eremina, T. A.; Furmanova, N. G.; Malakhova, L. F.; Okhrimenko, T. M.; Kuznetsov, V. A. *Kristallografia* **1993**, *38*, 236–240.
(26) Otinowski, Z.; Minor, W. *Methods Enzymol.* **1996**, *276*, 307–326.
(27) Altomare, A.; Cascarano, G.; Giacovazzo, C.; Guargliardi, A.; Burla, M. C.; Polidori, G.; Camalli, M. *J. Appl. Crystallogr.* **1997**, *27*, 435–442.
(28) Sheldrick, G. M. *SHELXL97*; University of Göttingen, Germany, 1997.
(29) Kuno, M.; Fromm, D. P.; Hamann, H. F.; Gallagher, A.; Nesbitt, D. J. *J. Chem. Phys.* **2001**, *115*, 1028–1040.
(30) Watkins, L. P.; Yang, H. *J. Phys. Chem. B* **2005**, *109*, 617–628. Zhang, K.; Chang, H. Y.; Fu, A. H.; Alivisatos, A. P.; Yang, H. *Nano Lett.* **2006**, *6*, 843–847.

species. Partially absorptive (A) and partially emissive (E) spectra are observed. Crystalline samples were studied between 80 and 165 K. We have not been able to observe a triplet signal from DCM in glasses.

The analysis of the TR-EPR spectra was based on a spin Hamiltonian consisting of the Zeeman and electron−electron dipolar term:

$$\hat{H} = \mu_B \mathbf{SgB} + \mathbf{SDS} \tag{1}$$

where **D** is the traceless dipolar tensor. For simplicity the principal directions of the **g** and **D** were assumed to be aligned, a good approximation in systems with vanishing g anisotropy. In the principal system of **D**, the dipolar tensor is diagonal and can be written as:

$$\hat{H}_{dsp} = D_X \hat{S}_X^2 + D_Y \hat{S}_Y^2 + D_Z \hat{S}_Z^2 \tag{2}$$

Whole crystals or individual growth sectors, removed with a wire saw and a razor blade ((010) is a perfect cleavage plane), were fixed with epoxy to quartz rods so that crystallographic axes well identified by crystal morphology were aligned with the rod's long axis. TR-EPR spectra were obtained at fixed rotation steps of crystal sectors or subsectors around the three crystallographic axes.

At each orientation of the magnetic field, the two transitions between the eigenstates $|-\rangle \rightarrow |0\rangle$ and $|0\rangle \rightarrow |+\rangle$ correspond to the two resonant fields $B_{res\pm}(\Omega)$, nearly symmetric in the high field approximation with respect to the center of the spectrum determined by the effective g value. The intensities of the two lines were proportional to the nonequilibrium population difference between the triplets sublevels $P_{\pm}(\Omega,B)$. Triplets produced through intersystem crossing (ISC), were expressed for each resonant field as linear combinations of populations of the zero-field states. The lines at low and high field were, respectively, mostly emissive and absorptive.

In each crystallographic plane the angular dependence of ΔB, the difference in resonant fields for the two transitions, were fit to the following:

$$\Delta \mathbf{B} = D_{ii} \cos^2 \theta + D_{jj} \sin^2 \theta + D_{ij} \sin \theta \cos \theta \tag{3}$$

derived by a first-order approximation.[31] By combining the three rotations around the three crystal axes, the fitting of the most intense lines established the six independent elements of the dipolar tensor.

Spectra of polycrystalline samples were simulated as:

$$I(B) = \sum_{\pm} \int G(B_{res\pm}(\Omega) - B) P_{\pm}(\Omega, B)\, d\Omega \tag{4}$$

where $G(B_{res\pm}(\Omega) - B)$ is a Gaussian line shape function centered at the calculated resonance fields of the two transitions for that particular orientation Ω and $P_{\pm}(\Omega,B)$ are the nonequilibrium population differences between the triplet sublevels.

Results

Bulk Spectroscopy. Absorbance of DCM in KAP showed three maxima at 408, 433, and 461 nm. Corresponding peaks for DCM in RAP were 404, 428, and 459 nm. DCM is highly dichroic in the single-crystal hosts, with the absorbing direction of the chromophore always oriented more closely to the [100]. Transition dipole moment orientations (θ) were computed according to: $\theta = \tan^{-1}(1.132 \cdot DR)^{-1/2}$, where the dichroic ratio ($DR = A_a/A_c$) was corrected for sample birefringence.[3] From the dichroic ratios, we computed orientations of electric dipole transition moments as 27° for KAP/DCM and as 22° or RAP/DCM from [100]. The fluorescence of DCM (Figure 3) was unstructured in ethanol with an emission maximum (λ_{max}) of 595 nm. In an aqueous solution saturated with KAP, λ_{max} shifted to 610 nm. In the crystal, there was a marked blue shift in the emission. It becomes structured with three peaks at 470, 507, and 545 nm. The fluoresence maxima of DCM in RAP crystals were 419, 460, 474, 493, and 545 nm. There was an extra, sharp peak (419 nm) in RAP/DCM wholly absent in KAP/DCM.

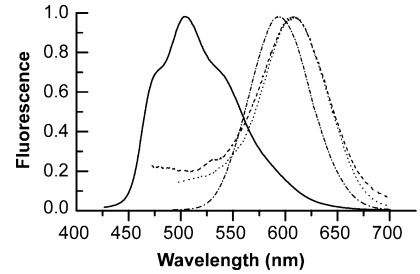

Figure 3. Normalized fluorescence spectra of DCM in solutions of ethanol (dash-dotted) and saturated KAP (dashed) as well as within a single crystal of KAP (solid), and redissolved crystals of KAP/DCM (dotted).

DCM Structure. DCM has two low-energy conformations differing in the orientation of the pyran ring, A and B in Figure 1. The minima are nearly equi-energetic. Both conformations have been considered in the literature.[32] Geometry optimization and excited-state calculations were performed within the Gaussian03 program suite using the Pople 6-31G* basis-set.[33] Ground-state geometries were optimized using the B3LYP functional and excited-state properties were determined using the time-dependent Hartree−Fock method. *Ab initio* and semiempirically computed energy differences are on the order of kT. Thus, both conformations A and B must be considered in evaluations of the ZFS tensor.

We determined the X-ray crystal structure of DCM in order to gain additional insight into its structure. The monoclinic cell parameters were a = 29.375(2) Å, b = 15.147(1) Å, c = 7.5187(7) Å, and β = 91.578(7)°. The space group was $C2/c$. The structure is unremarkable. It shows that in the solid state, DCM crystallizes in the A conformation (see Supporting Information, Figure S1).

Blinking Dynamics. Single molecules of DCM in KAP exhibited broad and energy-dependent orientational distributions.[3] To determine the impact of disperse orientations (i.e., local environments) on molecular photophysics we measured the blinking dynamics from individual molecules of DCM in KAP. Figure 4 presents an emission time trace of a representative single molecule analyzed with the change point detection algorithm.

Blinking dynamics in KAP/DCM were quantified in terms of on- and off-time distributions using thresholding. Continuous distributions of the on- and off-time probability densities ($P(\tau_{on/off})$) were derived from these data by dividing each value in the distribution by the average time to its nonzero nearest neighbors.[4c] The resulting logarithmic plots of $P(\tau_{on})$ and $P(\tau_{off})$ are shown respectively in a and b of Figure 5. Both $P(\tau_{on})$ and $P(\tau_{off})$ are well described with a power-law

(31) Atherton, N. M. *Principles of ESR*; Ellis Horwood and Prentice Hall: London, 1993.

(32) Van Tassle, A. J.; Prantil, M. A.; Fleming, G. R. *J. Phys. Chem. B* **2006**, *110*, 18989–18995. Yao, Y.-S.; Zhou, Q.-X.; Wang, X.-S.; Wang, Y.; Zhang, B.-W. *Adv. Funct. Mater.* **2007**, *17*, 93–100.

(33) Frisch, M. J.; et al. *Gaussian 03*, revision C.02; Gaussian, Inc.: Wallingford, CT, 2004.

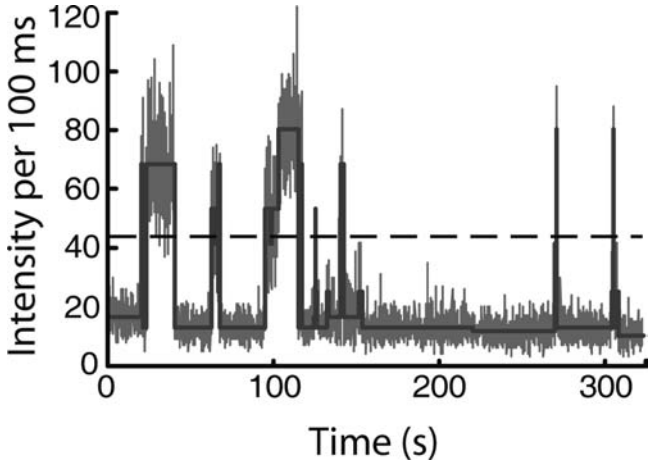

Figure 4. A representative blinking trace for a single molecule of DCM in KAP (gray line). The threshold employed to determine transitions between on- and off-events is shown (black dashed line). In addition, intensity trace determined using CPD (black solid line) is shown. While both analyses revealed power-law distributed on- and off-event durations, this comparison demonstrates that a single threshold discards some emissive periods, thereby affecting the overall statistics.

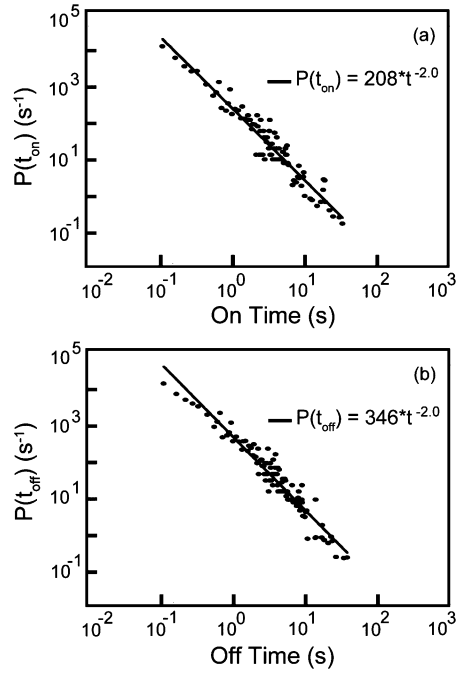

Figure 5. On- and off-time probability distributions in KAP/DCM determined using thresholding. Power-law exponents are 2.

of the form $P(\tau_{on/off}) = P_0\tau_{on/off}^{-m_{on/off}}$. On times and off times ranged from 0.05 s (the experimental temporal resolution) to 38.5 and 40.3 s, respectively. Best fits to the power-law function corresponding to $P_0(on) = 208$, $m_{on} = 2.0$, and $P_0(off) = 346$, $m_{off} = 2.0$ are plotted in Figure 5, respectively. For comparison, the power-law exponents observed for other systems including individual quantum dots and single molecules in heterogeneous environments range from $m \approx 1.4$ to 2.[33] The CPD method was employed for a number of emission traces and established that multiple statistically significant intensity states are observed; however, this analysis was not used to determine the power-law statistics. We have carried out a comparison between CPD and

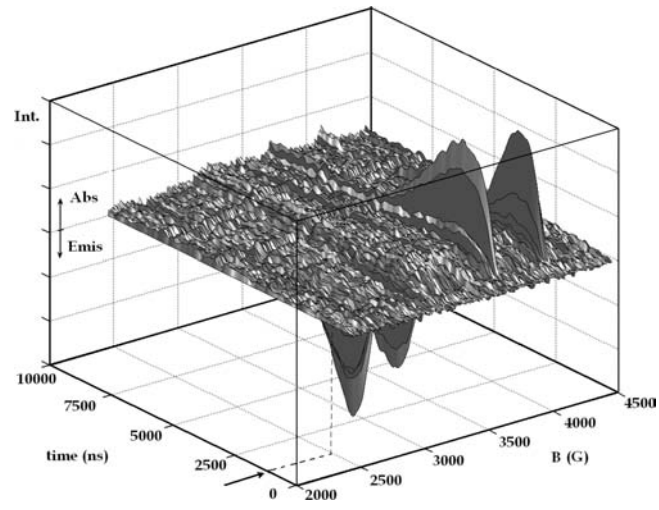

Figure 6. Example of a full transient surface at 80 K of a whole KAP/DCM crystal in the *ac* plane (−72° from *a*). Signal coming from triplets I and II are visible. An arrow indicates the arrival of the laser flash.

thresholding analysis methods for similar chromophores, violamine R and dichlorofluorcein, isolated in KAP. Although the power-law statistics differed between threshold and CPD analysis ($m = \sim 2$ to ~ 1.5 for both on and off times, respectively), power-law behavior was observed in using both techniques. It is anticipated that DCM/KAP exhibits similar behavior.

Zero-Field Splitting Tensors. One example of the shape of the EPR spectrum can be seen in Figure 6, where the time axis shows the signal evolution for different laser pulse delays. In these spectra, signals appear as a pair of lines. Each doublet corresponds to a DCM in a triplet state in a particular orientation inside the crystal. The centers of the doublets are isochronous for different orientations indicating a negligible *g*-tensor anisotropy. The number and intensities of the weaker lines vary with the sample and its orientation in the magnetic field. Only the two strong doublets can be followed in the three crystallographic planes in all the crystals, and the angular dependence of their splittings (Figure 7) gives the ZFS parameters of just two triplets, designated I and II. The principal values and directions of their fine tensors are reported in Table 1.

The unique orientation of each of the two triplets I and II is puzzling for the following reasons. In KAP crystals of *mm*2 symmetry, two magnetically equivalent sites are expected for rotations in the crystallographic planes in the space group of KAP, $Pca2_1$, becoming equivalent when the magnetic field is along one of the crystal axes. This implies that any fragment of such a hypothetical mixed crystal when rotated around the crystal axes should give symmetry-related TR-EPR lines, fitting two sets of curves as in eq 3, corresponding to the same values of D_{ii} and D_{jj}, and related by a sign change of D_{ij}. Instead, irrespective of sample orientation with respect to the magnetic field, we see just triplets I and II, each in a unique orientation.

The principal values of the two triplets are similar, but their difference well exceeds the experimental error (see Table 1). The direction cosines of the *Y* and *Z* principal axes of the two triplets indicate a misorientation by 6° from what would otherwise be a reflection operation across the *bc* plane. This misorientation can be appreciated in Figure 7 by comparing in each crystallographic plane the angular dependence of the splitting of the doublets for triplets I and II. The relative orientations of the two triplets with respect to the crystal-

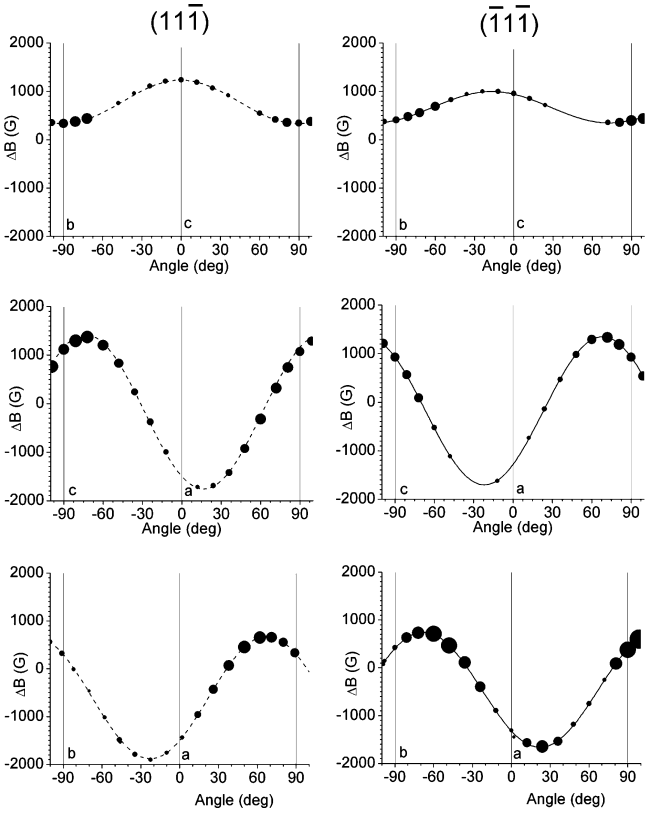

Figure 7. Angular dependence of the difference in resonance fields for DCM triplets in ($\bar{1}$1$\bar{1}$) and (11$\bar{1}$) growth sectors of KAP. The area of the circles is proportional to intensity; from top to bottom, rotations around *a*, *b*, and *c* crystallographic axes. Best fit calculated resonances based on eq 3 are shown (dotted lines for 11$\bar{1}$ and solid lines for $\bar{1}$1$\bar{1}$).

Table 1. Zero-Field Splitting Tensors

	$-D_{ii}$/gauss	direction cosines		
		a	*b*	*c*
($\bar{1}$1$\bar{1}$) triplet I	$X = -192(\pm5)$	−0.26	0.91	0.34
	$Y = -499(\pm5)$	−0.34	0.24	−0.91
	$Z = +694(\pm5)$	0.91	0.35	−0.24
(11$\bar{1}$) triplet II	$X = -222(\pm5)$	0.24	0.93	0.30
	$Y = -458(\pm5)$	0.41	0.19	−0.89
	$Z = +677(\pm5)$	0.88	0.33	−0.33

lographic axes are shown in Figure 8. Figure 1A shows the calculated orientation of the ZFS principal axes with respect to the π-system.

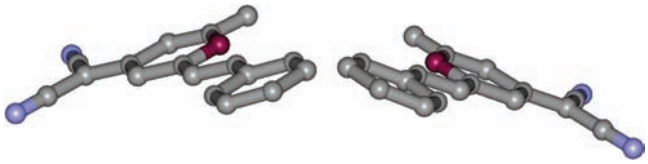

Figure 8. Orientation of $DCMH^+$ triplets in KAP viewed along the *b* axis. Only atoms carrying the π-system are shown. Approximate *ac* mirror symmetry is evident, but it is clear that the structure on the right is more foreshortened.

In order to further characterize this apparent loss of symmetry we partitioned KAP/DCM crystals into subvolumes corresponding to the ($\bar{1}$1$\bar{1}$) and (11$\bar{1}$) growth sectors related by mirror symmetry with respect to the *bc* plane (Figure 2). In this way, we were able to isolate the two main triplets, associating one with each of the respective sectors.

Triplet Lifetimes. Time evolution of EPR signals following laser excitation depends on the decay of the photoexcited triplet state to the ground state as well as other spin relaxation processes.[34] We approximated the decay rate of the triplet state by a single rate constant (k_T). The nonequilibrium spin populations of the triplet sublevels relax to the Boltzmann equilibrium for the lattice-induced spin transitions. We simplified the scheme of the spin relaxation considering only the two spin sublevels involved in the transition, with two slightly different rates for the upward and downward lattice-induced transitions, k_1 and $k_1 + k'$, respectively, due to the Boltzmann distribution at thermal equilibrium.

Within this scheme, the kinetic expression for the overall population difference, Δn, is as follows:

$$\Delta n(t) = (N_0\, e^{-k_T t}) \frac{k_1}{2k_1 + k'} \left[\frac{k'}{k_1} + 2 \cdot (1 - 2p)\, e^{-(2k_1 + k')t} \right] \quad (5)$$

where N_0 is the initial population of the two levels involved, and $p = N_{upper}/N_0$. Neglecting the small population difference at thermal equilibrium, $0 \le p \le 1$, where for $p = 0$ ($p = 1$) only the lower (upper) level is populated.

In Figure 9 we report the experimental and calculated time dependences of the emissive EPR signal of triplet I. For a decaying polarized EPR absorption signal it can be difficult to disentangle the contribution due to the spin relaxation from that due to the decay of the electronic excited state. Fortunately, this was possible by following the time evolution of the emissive signal and taking advantage of the comparable values of the spin−lattice time $T_1 = 1/(2k_1 + k')$ and of the triplet lifetime $\tau = 1/k_T$. The TR-EPR signal evolves in time from emission to absorption, passing through zero. Once it reaches the small positive value, corresponding to the spin populations at thermal equilibrium, it decays to zero. At 100 K we obtained $T_1 = 90\ \mu s$ and $\tau = 40\ \mu s$.

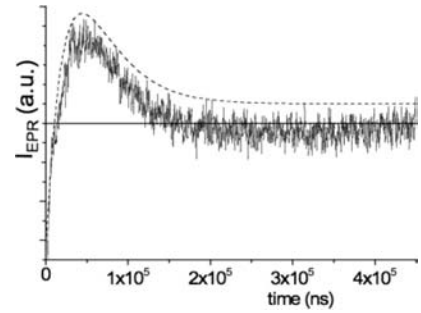

Figure 9. Experimental low-power (55 dB) initially emissive TR-EPR signal of triplet I at 100 K (solid line), and the calculated time dependences by eq 3 (dashed line).

The spin relaxation of TR-EPR signals are affected in general by a mixing of T_1 and T_2 processes, except at very low power when the T_1 relaxation is the most prominent.[35] An alternative to the continuous wave transient EPR signal is via electron spin echo. The echo is collected at varying times after the laser pulse. This method avoids T_2 mixing but has the disadvantage of a

(34) Dauw, X. L. R.; Poluektov, O. G.; Warntjes, J. B. M.; Bronsveld, M. V.; Groenen, E. J. J. *J. Phys. Chem. A* **1998**, *102*, 3078–3082.
(35) Furrer, R.; Fujara, F.; Lange, C.; Stehlik, D.; Vieth, H. M.; Vollmann, W. *Chem. Phys. Lett.* **1980**, *75*, 332–339.

lower sensitivity. The decay of the echo-detected, transient, emissive signal to zero was consistent with the continuous wave results.

Triplet EPR signals were recorded only up to 165 K; at higher temperatures the probability for intersystem crossing becomes less efficient than other processes. We analyzed the TR-EPR decays for $T > 100$ K as monoexponential functions with constant $k_{Tot} = 2k_1 + k' + k_T$. By assuming that the variation of the decay rate with the temperature remains linear to room temperature the corresponding triplet lifetime at room temperature is $\tau \approx 20-30$ μs. This assumption is sound for dyes in crystals, as changes in the triplet lifetimes with the temperature are mainly attributed to conformational dynamics.[36]

Discussion

Kinetic Ordering. In the analysis of mixed crystals, just as with inhomogeneously broadened spectral lines, we likewise have learned to parse averages. Becke[37] recognized that a polyhedral crystal is not a monolith but rather an assemblage of growth pyramids or growth sectors whose bases correspond to growth faces and whose coincident apexes mark the site of crystal nucleation. Shubnikov recognized that such pyramids would naturally be of reduced symmetry in the presence of suitable impurities 'feeding' the faces.[38] Therefore, the symmetry of the growth front has a major influence on crystal properties.

The essence of the growth desymmetrization phenomenon is as follows: Positions related by symmetry in the bulk of a crystal may be, and most often are, structurally and energetically nonequivalent on a growing surface. These differences give rise to an ordered distribution of structural units in the surface layer. The ordered distribution is then overgrown and buried in a metastable state. The crystal would have a lower free energy were the guests statistically distributed among bulk sites having the same potential energy. Because the metastable state can persist indefinitely because of the slow diffusion in solids, the crystal symmetry is reduced.[39]

Growth sectors often have distorted optical indicatrices as a consequence of unidirectional growth in any one sector. The refractive indices of sectors associated with growth faces of different forms usually differ in magnitudes and directions. One can say that symmetry-related faces often have the same 'eigenvalues' but different 'eigenvectors'. So-called 'optical anomalies' or anomalous linear birefringence provided the earliest evidence for symmetry reduction in mixed crystals,[40] but the average optical indicatrix does not cleanly differentiate between mechanisms of symmetry reduction. To do so, one would have to interrogate ostensibly symmetry-related sites independently. This can be done by rendering the sites magnetically nonequivalent in an applied magnetic field. Thus, we discover that the earliest evidence for kinetic ordering comes from EPR spectroscopy.

More than half a century ago, compounds with nonrandom distributions of impurities among nominally equivalent sites were revealed by electron paramagnetic resonance spectroscopy. These impurities include Gd^{3+} in synthetic corundum, Al_2O_3,[41] and Fe^{3+} in calcite,[42] Fe^{3+} in amethyst.[43] Nonequivalence of sites on crystal faces differentially occupied by impurities during growth was thus established but not explained. Detailed mechanisms were first considered in quartz,[44] zinc selenate,[45] and sodium kröhnkite ($Na_2Cd(SO_4)_3 \cdot 2H_2O$).[46]

In the aforementioned examples, the magnetic species were invariably metal ions. However, during the past 15 years we have seen a generalization of single-crystal matrix isolation illustrated by all sorts of complex molecules serving as analytes in simple single-crystal hosts.[47] To the best of our knowledge, growth desymmetrization by the tried and true method of EPR has not been demonstrated for magnetic *molecules*.

In the space group $Pca2_1$ with point group $mm2$ (C_{2v}), there are general crystallographic positions at (x, y, z), ($-x$, $-y$, $z+1/2$), ($x+1/2$, $-y$, z), ($-x+1/2$, y, $z+1/2$). For magnetic molecules statistically distributed among these sites, with the applied magnetic field along a general direction [xyz], we should observe four distinct dipolar splittings (doublets) in the EPR spectrum. With the field oriented in a principal plane along directions [$xy0$], [$x0z$], or [$0xy$], we should see only two doublets. With the field along one of the orthorhombic crystallographic axes, [$x00$], [$0y0$], [$00z$], the ZFS tensors are all similarly projected in the plane perpendicular to the applied field. We thus should see only a single doublet. However, under the constraints of kinetic growth perpendicular to $\{11\bar{1}\}$, the four sites need not be statistically occupied because they make different presentations on these asymmetric surfaces; while KAP has point symmetry $mm2$ (C_{2v}), the $\{11\bar{1}\}$ growth faces have symmetry 1 (C_1). Indeed, we observe only one of the four expected triplets in individual growth sectors.

Previously, we recorded the TR-EPR spectra of diaminoacridine in KAP crystals.[48] Data was taken from small, whole crystals. We failed to detect any kinetic ordering. Were it present, it might well have to be counterbalanced by averaging mirror-related growth sectors, thus mimicking mirror-related sites in a single growth sector. For DCM in KAP, because of the pathological dissymmetry between growth sectors that should be related by symmetry, the kinetic ordering was hard to miss.

There remains some substantive unfinished business: While the kinetic ordering within single growth sectors is comprehensible, the failure to observe mirror-related DCM triplets in mirror-related growth sectors is perplexing. We prepared crystals of RAP/DCM in order to establish whether the symmetry breaking observed in KAP/DCM was reproducible in a closely related substance. Indeed, we observed triplets oriented as I and

(36) Görner, H.; Kuhn, H. J. in *Adv. Photochem.*, Vol. 19 (Neckers, D. C.; Volman, D. H.; von Bünau, G. Eds.) John Wiley, New York, 1995, p 1−117.
(37) Becke, F. *Lotos* **1894**, 14.
(38) Shubnikov, A. V. *Sov. Phys. Crystallogr.* **1961**, *6*, 319–322.
(39) Vaida, M.; Shimon, L. J. W.; Weisinger-Lewin, Y.; Frolow, F.; Lahav, M.; Leiserowitz, L.; McMullan, R. K. *Science* **1988**, *241*, 1475–1479. McBride, J. M.; Bertman, S. B. *Angew. Chem., Int. Ed. Engl.* **1989**, *28*, 330–333. Gervais, C.; Hulliger, J. *Cryst. Growth Des.* **2007**, *7*, 1925–1935.
(40) Kahr, B.; McBride, J. M. *Angew. Chem., Int. Ed. Engl.* **1992**, *31*, 1–26. Shtukenberg, A.; Punin, Y. *Optically Anomalous Crystals* (Kahr, B. ed.) Springer, Dordrecht, 2007.
(41) Geschwind, S.; Remeika, J. P. *Phys. Rev.* **1961**, *122*, 757–761.
(42) Marshall, S. A.; Reinberg, A. R. *Phys. Rev.* **1963**, *132*, 134–142.
(43) Barry, T. I.; Moore, W. J. *Science* **1964**, *144*, 289290; Barry, T. M.; McNamara, P.; Moore, W. J. *J. Chem. Phys.* **1965**, *42*, 2599–2606.
(44) Tsinober, L, I.; Samoilovich, M. I. *Problems in Modern Crystallography* (Vainshtein, B. K.; Chernov, A. A. eds.) Nauka, Moscow, pp 207−218.
(45) Nizamutdinov, N. M.; Bulka, G. R.; Khasanova, N. M.; Shchepkin, V. D.; Vinokurov, V. M. *Sov. Phys. Crystallogr.* **1977**, *22*, 445–450.
(46) Vinokurov, V. M.; Bulka, G. R.; Nizamutdinov, N. M.; Khasanova, N. M. *Dokl. Akad. Nauk SSSR* **1977**, *237*, 1388–1391.
(47) Kahr, B.; Gurney, R. W. *Chem. Rev.* **2001**, *101*, 893–951.
(48) Barbon, A.; Bellinazzi, M.; Benedict, J. B.; Brustolon, M.; Fleming, S. D.; Jang, S.-H.; Kahr, B.; Rohl, A. L. *Angew. Chem., Int. Ed.* **2004**, *43*, 5278–5286. Bellinazzi, M.; Barbon, A.; Kahr, B.; Benedict, J. B.; Brustolon, M. *Phys. Chem. Chem. Phys.* **2006**, *8*, 379–385.

II in adjacent sectors that were not related by symmetry to one another. We noticed that some KAP crystals developed $(\bar{1}2\bar{1})$ and $(12\bar{1})$ facets in addition to $(\bar{1}1\bar{1})$ and $(11\bar{1})$; however, the relative areas of the mirror-related faces were rarely related to one another by mirror reflection. We surmised that the $\{12\bar{1}\}$ facets might give rise to one of the triplets while $\{11\bar{1}\}$ facets might give rise to the other. This hypothesis did not bear out the isolation of $\{11\bar{1}\}$ subvolumes from $\{12\bar{1}\}$ subvolumes by cleaving the crystals along (010).

The origin of the unexpected symmetry breaking must then be attributable to things unseen such as microtopography of growing crystals. While we know a great deal about the microtopography of the {010} faces of KAP,[49] to date the microtopographies of the other facets of KAP have not been characterized. Alternatively, the unexpected symmetry breaking may be attributable to unseen chiral impurities that differentially block enantiomorphous KAP docking sites. In chemistry, unexpected mirror symmetry breaking is observed from time to time. For instance, it was recently seen that D- and L-tyrosine had different solubilities in water.[50] The authors of this study reached for an extraordinary explanation, parity violating energy differences; however, Ockham[51] would search elsewhere, and other philosophers[52] reasonably ascribed the observations on tyrosine to undetected chiral impurities that can surely affect crystal growth and dissolution in small quantities.[53] Similar effects may well account for the differences seen herein.

Molecular Structure and Energy. The absorption and fluorescence spectra of DCM in KAP are markedly blue-shifted with respect to solution (Figure 3). DCM is a well-known red fluorophore;[54] however, the luminescent, doped KAP crystals are yellow-green. Such a blue shift previously has been observed from DCM in MCM-41 zeolite (but not zeolite Y).[21] Protonation of DCM at the amino nitrogen to give $DCMH^+$ truncates the conjugation path and would account in part for the blue shift. The calculated *ab initio* energies for DCM and $DCMH^+$ were 402 and 384 nm, respectively. While the solution pK_a of protonated DCM is undoubtedly smaller than that for the hydrogen phthalate anion, DCM is not at equilibrium in the crystal and it is not unusual to see protons in acid−base cocrystals on the "wrong" molecule, if judged from solution pK_a's alone.

Given the possibility of DCM protonation, we calculated the ZFS tensors for the triplet state of DCM and $DCMH^+$ in the A and B conformers according to the point dipole approximation[55] and spin densities from the AM1 method (Table 2).[56] Calculations of ZFS for dyes with heteroatoms are known to underestimate these parameters[48] by about 10−20%. However, in the present case the difference between calculated and experimental parameters for the triplet of DCM is too large to be attributed to the approximation of the calculation method. A more localized π system as $DCMH^+$ gives calculated parameters closer to the experiment, within the usual tolerance range. The $DCMH^+$ A conformer fits best. We therefore judge, on the basis of the optical blue shift and comparisons of calculated and measured ZFS tensors that $DCMH^+$ in the A conformation is the predominant species in the crystal.

Table 2. Calculated ZFS Tensor Principal Values

chromophore (conformation)	$-D_i$/gauss
DCM (A)	$X = -54$
	$Y = -57$
	$Z = +112$
DCM (B)	$X = -57$
	$Y = -59$
	$Z = +116$
$DCMH^+$ (A)	$X = -167$
	$Y = -388$
	$Z = +555$
$DCMH^+$ (B)	$X = -52$
	$Y = -414$
	$Z = +466$

Etiology of Blinking. Early in the brief history of single-molecule spectroscopy nonemissive periods (i.e., off times) were attributed to intersystem crossing to long-lived triplet states.[57] However, it was quickly recognized that in some systems, including DCM,[58] extremely long off times were not consistent with intersystem crossing rates; that is they were not attributable to the population and depopulation of an optically dark state with well-defined rate constants. The blinking statistics of single semiconductor quantum dots exhibit logarithmic ranges of on(off) times that are well fit to power laws.[59] Power-law statistics, requiring on(off) measurements spanning ≥3 orders of magnitude, are often precluded for single molecules by photobleaching.

We have taken the approach of studying the blinking dynamics of organic luminophores isolated in single crystals of KAP.[3,4,60] Single host crystals are ordered and restrict molecular translation and rotation. Oxygen impermeable crystalline matrices retard irreversible chromophore photooxidation. The enhancement in photostability provided by the crystal prolongs the time over which single emitters may be studied and, consequently, reveals a more complete picture of single-molecule blinking. Indeed, the blinking dynamics of single dye molecules (i.e., violamine R, dichlorofluorescein) in KAP followed power laws for both on and off times with exponents of $m_{on/off} \approx 1.5$.[4c] Here, power-law behavior was observed for single molecules of KAP/DCM, with $m_{on/off} = 2.0$ as shown in Figure 5.

In order to evaluate the role of triplets in power-law distributions, we performed TR-EPR measurements of heavily dyed KAP/DCM crystals. The TR-EPR triplet-state decay of DCM was well behaved and first order, with a room temperature lifetime of ∼25 μs. On the other hand, we have observed single

(49) Price, R.; Ester, G. R.; Halfpenny, P. J. *Proc. R. Soc. London, Ser. A* **1999**, *455*, 4117–4130.
(50) Shinitzky, M.; Nudelman, F.; Barda, Y.; Haimovitz, R.; Chen, E.; Deamer, D. W. *Origins Life Evol. Biosys.* **2002**, *32*, 285–297.
(51) Hoffman, R.; Minkin, V. I.; Carpenter, B. K. *Bull. Soc. Chim. Fr.* **1996**, *113*, 117–130.
(52) Lahav, M.; Weissbuch, I.; Shavit, E.; Reiner, C.; Nicholson, G. J.; Schurig, V. *Origins Life Evol. Biosys.* **2006**, *36*, 151–170. See also rebuttal: Shinitzky, M. *Origins Life Evol. Biosys.* **2008**, *38*, 271.
(53) Nyvlt, J.; Ulrich, J. *Admixtures in Crystallization*; Wiley-VCH: Weinheim, 1995.
(54) Jung, B.-J.; Yoon, C.-B.; Shim, H.-K.; Do, L.-M.; Zyung, T. *Adv. Funct. Mater.* **2001**, *11*, 430–434.
(55) Visser, J.; Groenen, E. J. J. *Chem. Phys. Lett.* **2002**, *356*, 43–48.
(56) Stewart, J. J. P. *MOPAC* (2002) Fujitsu Ltd, Tokyo, Japan.
(57) Vogel, M.; Gruber, A.; Wrachtrup, J.; von Borczyskowski, C. *J. Phys. Chem.* **1995**, *99*, 14914–14917. Veerman, J. A.; Garcia-Parajo, M. F.; Kuipers, L.; van Hulst, N. F. *Phys. Rev. Lett.* **1999**, *83*, 2155–2158. Köhn, F.; Hofkens, J.; Gronheid, R.; Van der Auweraer, M.; De Schryver, F. C. *J. Phys. Chem. A* **2002**, *106*, 4808–4814. Kulzer, F.; Kummer, S.; Basché, T.; Brauchle, C. *J. Inf. Rec.* **1996**, *22*, 567–572.
(58) von Borczyskowski, C.; Cichos, F.; Martin, J.; Schuster, J.; Issac, A.; Brabandt, J. *Eur. Phys. J. Special Top.* **2007**, *144*, 13–25.
(59) Cichos, F.; von Borczyskowski, C.; Orrit, M. *Curr. Opin. Colloid Interface Sci.* **2007**, *12*, 272–284.
(60) Bullard, T.; Wustholz, K. L.; Bott, E. D.; Robertson, M.; Reid, P. J.; Kahr, B. *Cryst. Growth Des.* **2009**, *9*, 982–990.

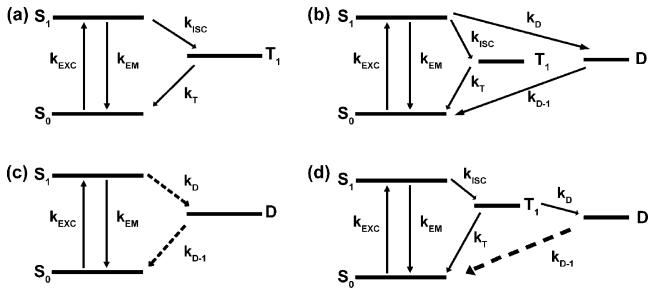

Figure 10. Schematic energy-level diagrams for blinking consisting of an electronic ground state (S_0), first excited singlet state (S_1), first triplet state (T_1), and dark state (D) with corresponding rate constants: (a) triplet blinking, (b) triplet and dark-state blinking, (c) distributed kinetics, (d) dark-state population via the triplet state (adapted from ref 10). Dotted lines represent distributed rates.

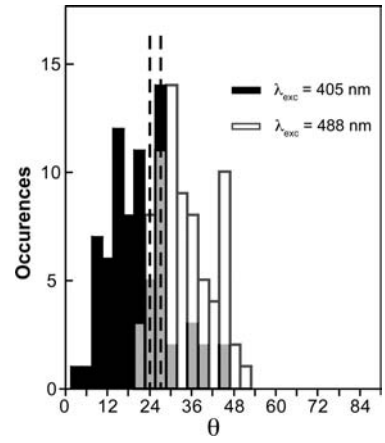

Figure 11. Orientational distributions of KAP/DCM obtained with 488-nm (white) and 405-nm (black) excitation. Overlapping region is shown in gray. *Z* eigenvectors for EPR tensors I and II are indicated as dotted lines at 24° and 28°, respectively.

DCM molecules with off times as long as 40 s (Figure 5). The probability of a common 10-s off event occurring for a 25-μs triplet lifetime is exceedingly small ($\sim 10^{-170,000}$). It is well-known that, for systems where population and depopulation of the triplet state is responsible for fluorescence intermittency (Figure 10a), the on(off)-time distributions are described by exponential functions reflecting the rate constants for intersystem crossing and triplet-state decay, respectively. This reiterates the fact that power-law statistics over several decades in time are inconsistent with the simple population and depopulation of a triplet state.

Previous attempts to model the complex blinking kinetics for both quantum dots and organic dyes have implemented three- and four-state systems presented in b−d of Figure 10. For a system wherein blinking occurs through a triplet state as well as a dark state (10b), the population and depopulation of two nonemissive states are expected to follow biexponential kinetics in the on(off)-time probability distributions. To account for power-law behavior, however, more complexity is required. For example, Figure 10c presents the distributed kinetics model, where the rate constants to and from the dark state are disperse.[61−63] Previously, we successfully employed Monte Carlo simulations based on distributed kinetics to model power-law behavior for single molecules in KAP.[4a,c] Lastly, Figure 10d presents a four-state system wherein population of the dark state is mediated by the triplet state. Applying this model to rhodamine 6G in a polymer, Zondervan et al. showed that first-order kinetics are insufficient for reproducing single-molecule dynamics. They presumed a distributed off rate for the dark-state exit channel resulting from a variety of photoelectron transfer sites. This interpretation was supported by the observation of an unstructured $g = 2$ signal in the EPR spectrum, characteristic of a radical.[10] In contrast, we did not observe in KAP/DCM any signatures in the EPR spectrum consistent with radical formation, demonstrating that electron transfer is also not responsible for the blinking dynamics in our system.

We did observe *bona fide* triplet states, and we thoroughly characterized their ZFS tensors and lifetimes by TR-EPR. While heavily dyed crystals suitable for EPR are not precisely the same objects as lightly doped crystals suitable for single-molecule studies,[60] in both cases the dye molecules are remotely separated from one another in the crystal. Nevertheless, the time dependence of the EPR data and the blinking dynamics cannot be reconciled with one another. This undermines our ability to tacitly assign the dark states responsible for single-molecule blinking to photoexcited triplets.

Nevertheless, it is reassuring to discover that the grossest structural information obtainable from single-molecule spectroscopy and EPR are in splendid accord. Figure 11 shows a histogram of the orientations of the $DCMH^+$ transition moments obtained by measuring the excitation dichroism. The bimodal distribution results from two different excitation wavelengths indicating some correlation between energy and orientation. Superimposed are dotted lines at 24° and 28° that indicate the directions of the Z-eigenvector of $DCMH^+$ triplets I and II, respectively.

Summary

To date there have been hundreds of publications that associate single-molecule dark states with photoexcited triplet states. However, to the best of our knowledge the kinetics of dark states and well-characterized triplet states rarely have been compared. Here, both the eigenvalues and eigenvectors of the ZFS tensors of photoexcited triplet states of KAP/DCM were determined. ZFS tensors do more to define the electronic structure of photoexcited triplets than most any other quantity. To our knowledge, KAP/DCM is the only chemical system in which molecules have been well characterized in their triplet states and in their individual dark states. This work highlights the utility of single-crystal matrix isolation for the characterization of single-molecule blinking dynamics. Were it not for the enhanced photostability afforded by the crystal environment, power-law statistics of single-molecule photoblinking may not have been detected. From the time constants associated with the decay of the triplet and the decay of the dark states it is clear that no single dynamical process can explain both sets of data, confirming that we must look beyond photoexcited triplets in the interpretation of dark states characterized by power laws. In addition, the EPR results establish that electron transfer cannot be responsible for dark state production in

(61) Molski, A.; Hofkens, J.; Gensch, T.; Boens, N.; Schryver, F. D. *Chem. Phys. Lett.* **2000**, *318*, 325–332.
(62) Molski, A. *Chem. Phys. Lett.* **2000**, *324*, 301–306.
(63) Yeow, E. K. L.; Melnikov, S. M.; Bell, T. D. M.; Schryver, F. D.; Hofkins, J. *J. Phys. Chem. A* **2006**, *110*, 1726–1734.

KAP/DCM. Yet another process must be responsible for blinking in this system.

One potential explanation is proton transfer resulting in transitions between the DCM and $DCMH^+$ protonation states of the chromophore. Proton transfer has not been included in the canon of blinking etiology since the energetic barriers to proton transfer were considered too small to account for dynamics on typical blinking time scales (ms to s). However, the environment provided by KAP may provide for a proton-transfer potential-energy landscape that makes proton transfer a viable mechanism for blinking. Other possible explanations for complex blinking dynamics include *cis*−*trans* photoisomerism and TICT state formation.[16,17] For example, the observation of long on and off times is consistent with the hypothesis that *cis*−*trans* isomerization is energetically unfavorable in the crystal environment. Alternatively, CPD analysis of the blinking dynamics of single DCM molecules revealed multiple, statistically significant emissive states (Figure 4), consistent with the TICT hypothesis. That is, upon photoexcitation DCM is promoted to a locally excited state (S_1) and may undergo intramolecular charge transfer to produce the most favored charge-separated state (S_2), depending on the polarity of the local environment. Indeed, single-molecule orientation measurements revealed that the local crystal environments are dispersive. Overall, the work presented here has demonstrated that photoinduced triplet states cannot be singularly responsible for dark state production. Other mechanisms have yet to be established.

Acknowledgment. B.K. acknowledges NSF Grant CHE-0349882. P.J.R. thanks the NSF for support of this work through the Center on Materials and Devices for Information Technology Research (DMR-0120967). K.L.W. was a NSF-IGERT and University Initiative Funded fellow, supported by the Center for Nanotechnology at the University of Washington (DGE-0504573). M.B. acknowledges financial support by the University of Padova.

Note Added after ASAP Publication. The uncorrected proof version of this article was published ASAP on July 22, 2009. The corrected version was published July 29, 2009.

Supporting Information Available: X-ray crystallographic data in CIF format. This material is available free of charge via the Internet at http://pubs.acs.org.

JA903284Y